Insight into binding of phosphodiesterase-9A selective inhibitors by crystal structures and mutagenesis

Huanchen Wang[1,¶], **Xuan Luo**[1,2,¶], **Mengchun Ye**[1], **Jing Hou**[2], **Howard Robinson**[3], and **Hengming Ke**[1,2,*]

[1] Department of Biochemistry and Biophysics and Lineberger Comprehensive Cancer Center, The University of North Carolina, Chapel Hill, NC 27599-7260, USA

[2] Structural Biology Lab, School of Pharmaceutical Sciences, Sun Yat-sen University, Guangzhou, 510275, China

[3] Biology Department, Brookhaven National Laboratory, Upton, NY 11973-5000, USA

Abstract

PDE9 inhibitors have been studied as therapeutics for treatment of cardiovascular diseases, diabetes, and neurodegenerative disorders. To illustrate the inhibitor selectivity, the crystal structures of the PDE9A catalytic domain in complex with the enantiomers of PDE9 inhibitor 1-(2-chlorophenyl)-6-(3,3,3-trifluoro-2-methylpropyl)-1*H*-pyrazolo[3,4-*d*]pyrimidine-4(5*H*)-one ((R)-BAY73-6691 or (S)-BAY73-6691, **1r** or **1s**) were determined and mutagenesis was performed. The structures showed that the fluoromethyl groups of **1r** and **1s** had different orientations while the other parts of the inhibitors commonly interacted with PDE9A. These differences may explain the slightly different affinity of **1r** (IC_{50} = 22 nM) and **1s** (IC_{50} = 88 nM). The mutagenesis experiments revealed that contribution of the binding residues to the inhibitor sensitivity varies dramatically, from a few of folds to three orders of magnitude. On the basis of the crystal structures, a hypothesized compound that simulates the recently published PDE9 inhibitors was modeled to provide insight into the inhibitor selectivity.

Keywords

Phosphodiesterase-9; crystal structure; automatic docking; inhibitor selectivity; mutagenesis

The second messengers adenosine and guanosine 3′, 5′-cyclic monophosphate (cAMP and cGMP) mediate the response of cells to a wide variety of hormones and neurotransmitters and modulate many metabolic processes, including cardiac and smooth muscle contraction, steroid hormone function, platelet aggregation, apoptosis, leukocyte migration, adrenal hyperplasia, inflammation, axon guidance and regeneration, memory, and circadian regulation.[1–7] The signaling of cAMP and cGMP *in vivo* is mainly involved in three types of enzymes: cyclases, phosphodiesterases, and kinases. Phosphodiesterases (PDEs) are the sole enzymes hydrolyzing cellular cyclic nucleotides and thus play pivotal roles in the physiological processes involving the nucleotide signaling pathways. Human genome contains 21 PDE genes that are categorized

into 11 families and encode over 100 isoforms of proteins via alternative mRNA splicing.[8–10]

PDE9 was first reported in 1998 and is cGMP-specific with Km of 70 – 390 nM and Vmax of 0.96 – 4.9 μmol/min/mg.[11–14] Since cGMP acts as a feed-forward mediator to enhance glucose-stimulated insulin secretion and sensitivity and also has an anti-apoptotic effect in beta cells, [15] control on cellular cGMP would represent a new direction for treatment of diabetes. For the specific activity of PDE9 in hydrolysis of cGMP,[16–18] PDE9 selective inhibitors have been studied as therapeutics for the treatments of the insulin-resistance syndrome,[19] cardiovascular diseases,[20] type 1 and 2 diabetes,[19, 21, 22] and obesity.[23] More recently, for its high expression in brain,[24] PDE9 has been shown to be a potential target for treatment of memory deficits that are associated with aging and neurodegenerative disorders such as Alzheimer's disease.[25–28]

The crystal structures of PDE9A in complex with non-selective inhibitor 3-isobutyl-1-methylxanthine (IBMX) or substrate cGMP have been reported,[14, 29] but no structures of PDE9 in complex with selective inhibitors are available. Lack of structural information is apparently an obstacle for discovery of PDE9 inhibitors and may explain why only few PDE9 selective inhibitors are available at present.[22, 30] The first published PDE9 selective inhibitor was 1-(2-chlorophenyl)-6-(3,3,3-trifluoro-2-methylpropyl)-1*H*-pyrazolo[3,4-*d*]pyrimidine-4 (5*H*)-one (**1**, BAY73-6691, Fig. 1), which has an IC$_{50}$ of 55 nM for PDE9 and shows ability to improve learning and memory in rodents.[27, 30] However, it remains unknown how inhibitor **1** selectively binds PDE9 and if one of its enantiomers is more effective than another. Reported here are the crystal structures of the PDE9A catalytic domain in complex with the enantiomers of **1** (**1r** and **1s**) and the kinetics of the wild type and mutant PDE9A to provide insight into the selectivity of PDE9 inhibitors.

Results

Structural asymmetry of two PDE9A catalytic domains in the crystals

PDE9 inhibitor **1** possesses a chiral center and thus has (R)- and (S)-enantiomeric configurations that are respectively abbreviated as **1r** and **1s** (Fig. 1). The structures of the PDE9A2 catalytic domain (residues 181–506) in complex with **1r** or **1s** were determined at 2.5 and 2.7 Å resolutions and refined to R-factor/R-free of 0.223/0.245 and 0.230/0.258, respectively (Table 1). Residues 187 to 505 of these structures were traced without ambiguity. The structures of the PDE9A2-**1** complexes consist of sixteen helices and two divalent metal ions (Fig. 2), which are folded into a topology similar to those of other PDE families.[31]

The asymmetric units of the PDE9A-**1r**/**1s** crystals contain two molecules of the PDE9A2 catalytic domain, the same as the previously reported structures of PDE9-IBMX and PDE9-cGMP.[14, 29] The superposition of chain A over chain B within each PDE9 structure by using all residues yielded root-mean-squared deviations (RMSD) of 0.55, 0.60, 0.65, and 0.72 Å, respectively for the Cα atoms of PDE9A in complex with cGMP,[29] IBMX,[14] **1r**, and **1s**. When the same chains in the different PDE9 structures were compared, the cross superposition yielded RMSDs of 0.35 to 0.43 Å. These numbers probably indicate conformational differences of the two molecules within the same structures. Careful examination of the structure comparison showed that three regions at residues 432–435, 440–446, and 495–505 had deviations larger than 2 times the average. Because residues 432–435 and 495–505 are distant from the inhibitor binding, it is unclear whether their positional changes are due to the inhibitor binding or the crystallographic packing. However, the movement of residues 440–446 appears to be biologically relevant. Residues 440–446 formed a 3$_{10}$ helix and had the shifts of 2 to 3 times the average for their Cα atoms in the structures of PDE9A in complex with IBMX, cGMP, **1r**, and **1s**. The unanimous shift of the helix in all the four structures may be the consequence of its direct interaction with the ligands. However, it is not clear if this asymmetric change of

the fragment implies an allosteric mechanism of the catalysis. The unliganded structure of PDE9 is needed for further illustration.

Subtle difference in the enantiomer binding to PDE9A

The complexes of PDE9A-**1r** and PDE9A-**1s** were prepared by soaking the PDE9A-IBMX cocrystals[14] in the inhibitor solutions. Since non-selective inhibitor IBMX has very weak affinity with PDE9A (IC$_{50}$ >200 μM),[12, 14] inhibitors **1r** and **1s** (IC$_{50}$ = 22 and 88 nM, respectively) were found to completely replace IBMX in the crystals by the soaking experiments, as shown by the electron density (Fig. 2).

Enantiomers **1r** and **1s** bind to the active site of PDE9 in a similar pattern (Fig. 2). The configurations of both enantiomers can be resolved without ambiguity, as shown by the electron density maps of both (Fo-Fc) and (2Fo-Fc). The residues for binding of the inhibitors show significant variation across PDE families (Table 2), implying a possibility to design PDE9 selective inhibitors. The pyrazolopyrimidine rings of 1r and 1s have common interactions with the PDE9A residues. They stack against Phe456 and also contact via van der Waals' interactions with residues Ile403, Asn405, and Leu420. The O$_4$ and N5 atoms of pyrimidine of both **1r** and **1s** form two hydrogen bonds with the side chain of the invariant Gln453 (Fig. 2). In addition, the chlorobenzyl groups of both enantiomers commonly contact mainly via hydrophobic interaction with residues His252, Met365, Leu420, Tyr424, and Phe456. However, trifluoromethyl groups of **1r** and **1s** show different orientations and interactions, although they interact with the same set of residues Leu420, Leu421, Tyr424, Phe441, Ala452, Gln453, and Phe456 (Fig. 2). Enantiomer **1s** makes four and five van der Waals' interactions respectively with Tyr424 and Phe441, while **1r** has only one and two interactions with these residues. On the other hand, **1r** makes five interactions with Leu420, but **1s** has only two. These different contacts may explain their slightly different affinity, as discussed below.

Mutagenesis reveals quantitative contribution of the binding residues

To evaluate the contribution of individual residues to the inhibitor binding, the following seven residues that directly interact with the inhibitors were mutated to alanine: Met365, Ile403, Leu420, Tyr424, Phe441, Gln453, and Phe456. The binding residue His252 was not studied because His252 has been proposed to serve as a general acid for the catalysis and its mutation would abolish the catalytic activity.[29, 32] The inhibition of **1r** and **1s** on the catalytic activities of wild type PDE9A2 and its mutants were measured (Table 3 and Fig. 3). The enantiomer **1s** had an IC$_{50}$ of 88 nM for the wild type PDE9A, which is 4 times less potent than **1r** (22 nM). Among the mutants, M365A and F441A showed about 2-fold changes on inhibitory sensitivity and thus appeared to be least important for binding of the inhibitors. The mutants of I403A, L420A and Y424A had 6- to 9-fold changes on the IC$_{50}$ values, suggesting their moderate roles in the inhibitor binding. Most dramatic changes were produced by the mutations of Gln453 and Phe456 to alanine, which made a loss of about three orders of magnitude of sensitivity, indicating their important roles for inhibitor binding. However, due to the invariance of Gln453 and the conservation of Phe456, they unlikely play critical roles in selective recognition of inhibitors. Instead, the other binding residues that show variation across PDE families (Table 2) should be critical for the inhibitor selectivity. For example, Tyr424 that is mutated to phenylalanine in most PDE families except for PDE8, could contribute a unique hydroxyl group for hydrophilic interaction and would be valuable for design of PDE9 selective inhibitors. In addition, Leu420 and Ile403 that show conserved mutation to valine, isoleucine or leucine in other PDE families (Table 2) may generate slightly different shape and size of the binding pockets and are thus important for the inhibitor binding.

Discussion

PDE9 inhibitors have been shown to be potential for treatment of cardiovascular diseases, [20] type 1 and 2 diabetes,[19, 21, 22] obesity,[23] and neurodegenerative disorders.[25–28] However, there are only a few of PDE9 selective inhibitors published today. Lack of structural information is apparently one of reasons for slow progress in discovery of PDE9 inhibitors. The crystal structures of PDE9 in complex with the **1r** and **1s** enantiomers reveal detailed interactions of the inhibitors, and are thus helpful with design of new PDE9 inhibitors. The structures show that the pyrazolopyrimidine rings of the **1r** and **1s** enantiomers form hydrogen bonds with Gln453 and stack against Phe456. Since these interactions are two characteristics of inhibitor binding in almost all PDE families, [14, 33–35] the pyrazolopyrimidine ring can be taken as a scaffold for design of new PDE9 inhibitors. In consideration of modification of pyrazolopyrimidine, the O_4 and N_5 atoms of pyrimidine form two hydrogen bonds with the invariant Gln453 in a pattern directly comparable with the binding of sildenafil and vadenafil, [35] and are thus valuable to be reserved. Among the other positions of pyrazolopyrimidine, atoms 1 and 6 seem to be available for attachment of substitution groups because they face an open space. An example of the design is shown in Fig. 4, and is basically equivalent to the mother compound of the inhibitors recently reported by Pfizer's group.[22] For position #1, a substitution group with medium size, such as an isopropyl (Fig. 4), could be attached to fit the hydrophobic environment that is constituted with Ile403 and Met365. Since this environment is neighbored to the metal binding pocket, a bigger substitution group with a hydrophilic atom might be considered to interact with the hydrophilic metal pocket. In general, the substitution at position #1 is predicted to improve the affinity of the inhibitors, but only the hydrophobic interaction may impact the inhibitor selectivity due to variation of Met365 and Ile403 across PDE families (Table 2).

Around position #6 is the subpocket, where the trifluoromethyl groups of the **1r** and **1s** enantiomers are located but not fully occupied (Fig. 4). This pocket comprises of Leu420, Leu421, Tyr424, Phe441, Ala452 and Gln453. Since these residues are conservatively mutated across PDE families (Table 2), the pocket is predicted to have slightly different shapes and sizes in the PDE families and may thus contribute to the inhibitor selectivity. This idea is supported by the observation that the trifluoromethyl groups of the **1r** and **1s** enantiomers have significantly different IC_{50} values although they occupy the similar pocket, and also by the fact that the mutation of the binding residues changes inhibitor sensitivity. In consideration of hydrophobicity and size of the pocket, a six-membered or even bigger ring could be fitted to improve the affinity and selectivity of inhibitors. An example is a benzyl ring fitting to the pocket (Fig. 4). It is interesting to note that the *ortho*-position of the modeled benzyl group, which is marked as R in Fig. 4, orients towards the molecular surface, implying that a large substitution group can be attached to this position. Although this prediction matches with the series of the recently reported PDE9 inhibitors,[22] the benzyl model neither perfectly fits the pocket (Fig. 4B), nor fully uses the existence of Tyr424 that may provide a unique hydroxyl group for the improvement of selectivity. This argument is strengthened by the observation that the Y748F mutation of PDE8A1 increased the sensitivity of PDE8 to the inhibitors of other PDE families.[36] In short, the pocket identified by the structural and kinetic studies in this report may be valuable for design of PDE9 selective inhibitors.

Material and Methods

Protein expression and purification of the PDE9A2 catalytic domain

The catalytic domain of the wild type human PDE9A2 (GenBank number BC009047) was purchased from American Type Culture Collection and subcloned following the protocol described previously.[14] The coding region for expression of residues 181–506 of PDE9A2 was amplified by PCR. The oligonucleotide primers that contain the restriction sites of NdeI and

XhoI were designed for amplification of the desired genes of the wild type PDE9A2 and its mutants. The amplified PDE9A2 cDNAs and the expression vector pET15b were separately digested by the restriction enzymes NdeI and XhoI, purified with agarose gel, and then ligated together with T4 DNA ligase.

PDE9A2 mutants of M365A, I403A, L420A, Y424A, F441A, Q453A, and F456A were derived from pET15b-PDE9A2. Site-directed mutagenesis was carried out by following a two-step PCR procedure. In the first round, two separate PCRs by using each primer were performed to amplify the single-strand cDNA that contains the expression vector and the PDE9A mutant. The products from the first round were then combined, annealed together, and amplified in the presence of Pfu Turbo polymerase (Stratagene). The mutation products of PCR were treated with DpnI endonuclease to eliminate the methylated parental DNA templates. All mutants were confirmed by sequencing plasmid DNAs.

The protein purification of the wild type and mutants of PDE9A used the similar protocols as described by Huai et al.[14] Briefly, the resultant plasmids pET-PDE9As were transferred into *E. coli* strain BL21 (Codonplus) for overexpression. The *E. coli* cells carrying pET-PDE9A plasmids were grown in LB medium at 37°C to absorption A600 = 0.7 and then 0.1 mM isopropyl β-D-thiogalactopyranoside was added for further growth at 15°C overnight. Recombinant PDE9A2 was purified by the chromatographic columns of Ni-NTA affinity (Qiagen), Q-Sepharose (GE Healthcare), and Sephacryl S300 (GE Healthcare). A typical batch of purification yielded 20–100 mg PDE9A2 from a 2-liter cell culture. The PDE9A2 proteins had purity greater than 95% as shown by SDS-PAGE.

Enzymatic assay

The enzymatic activities of the PDE9A2 (181–506) catalytic domain and its mutants were assayed by incubating the enzymes with 100 μl of reaction mixture of 50 mM Tris-HCl (pH 7.8), 10 mM $MgCl_2$, 0.5 mM DTT, and ^{3}H-cGMP (20,000–40,000 cpm/assay, GE Healthcare) at room temperature for 15 min. The reactions were terminated by addition of 200 μl 0.2 M $ZnSO_4$ and $Ba(OH)_2$. The reaction product ^{3}H-GMP was precipitated out while unreacted ^{3}H-cGMP remained in the supernatant. After centrifugation, the supernatant was added into 3.5-ml liquid scintillation cocktail (ScintiSafe Plus™ 30%, Fisher Scientific) and the radioactivity was measured by a LKB RackBeta 1214 counter. For measurement of IC_{50}, 16 concentrations of inhibitors were used in the presence of 30 nM substrate. The enzyme concentration that hydrolyzed up to 70% cGMP was chosen for each inhibition assay. The hydrolysis rate had a linear relationship with the enzyme concentration and the reaction time until 80% substrate was converted to product. Each experiment was repeated three times. The IC_{50} values are the concentration of inhibitors when 50% activities of the enzymes were inhibited.

Inhibitors, crystallization, and structure determination

Enantiomer **1s** was purchased from Sigma-Aldrich (catalog number B3561) and **1r** was a kind gift of Bayer Healthcare, Germany. Crystals of the PDE9A2-**1r** and PDE9A2-**1s** complexes were prepared by soaking PDE9A2-IBMX co-crystals in the buffer of 0.1 M HEPES (pH 7.5), 3.6 M sodium formate, and 2 mM **1r** or **1s** at 25°C for 3 days. The PDE9A2-IBMX crystals were grown by (1) mixing 10–15 mg/mL PDE9A2 catalytic domain (amino acids 181–506) with 2 mM IBMX in a buffer of 50 mM NaCl, 20 mM Tris. HCl (pH 7.5), 1 mM β-mercaptoethanol, 1 mM EDTA, and (2) vapor diffusion (hanging drop) at 4°C. The protein drops contained 2 μl PDE9A2-IBMX complex and 2 μl well buffer of 0.1 M HEPES (pH 7.5) and 3.0 M sodium formate. The well buffer plus 20% glycerol was used as the cryo-solvent to freeze the crystals in liquid nitrogen. Diffraction data were collected on beamline X29 at Brookhaven National Laboratory (Table 1) and processed by program HKL.[37] The structures of PDE9A2-**1r** and PDE9A2-**1s** were solved by molecular replacement program AMoRe,[38]

using the PDE9A catalytic domain[14] as the initial model. The atomic model was rebuilt by program O[39] against the electron density map that was improved by the density modification package of CCP4. The structure was refined by CNS.[40]

Acknowledgments

Abbreviations

|	
PDE	phosphodiesterase
PDE9A	phosphodiesterase-9A
(R)- and (S)-BAY73-6691	(R)- and (S)-1-(2-chlorophenyl)-6-(3,3,3-trifluoro-2-methylpropyl)-1*H*-pyrazolo[3,4-*d*]pyrimidine-4(5*H*)-one
cAMP	adenosine 3′, 5′-cyclic monophosphate
cGMP	guanosine 3′, 5′-cyclic monophosphate
IBMX	3-isobutyl-1-methylxanthine

References

1. Houslay MD. Adaptation in cyclic AMP signaling processes: a central role for cyclic AMP phosphodiesterases. Cell Develop Biol 1998;9:161–167.

2. Antoni F. Molecular diversity of cyclic AMP signaling. Front Neuroendocrin 2000;21:103–132.

3. Zaccolo M, Movsesian MA. cAMP and cGMP signaling cross-talk: role of phosphodiesterases and implications for cardiac pathophysiology. Circ Res 2007;100:1569–1578. [PubMed: 17556670]

4. Piper M, van Horck F, Holt C. The role of cyclic nucleotides in axon guidance. Adv Exp Med Biol 2007;621:134–143. [PubMed: 18269216]

5. O'Neill JS, Maywood ES, Chesham JE, Takahashi JS, Hastings MH. cAMP-dependent signaling as a core component of the mammalian circadian pacemaker. Science 2008;320:949–953. [PubMed: 18487196]

6. Horvath A, Stratakis CA. Unraveling the molecular basis of micronodular adrenal hyperplasia. Curr Opin Endocrinol Diabetes Obes 2008;15:227–233. [PubMed: 18438169]

7. Hannila SS, Filbin MT. The role of cyclic AMP signaling in promoting axonal regeneration after spinal cord injury. Exp Neurol 2008;209:321–332. [PubMed: 17720160]

8. Bender AT, Beavo JA. Cyclic nucleotide phosphodiesterases: molecular regulation to clinical use. Pharmacol Rev 2006;58:488–520. [PubMed: 16968949]

9. Omori K, Kotera J. Overview of PDEs and their regulation. Circ Res 2007;100:309–327. [PubMed: 17307970]

10. Conti M, Beavo J. Biochemistry and physiology of cyclic nucleotide phosphodiesterases: Essential components in cyclic nucleotide signaling. Ann Rev Biochem 2007;76:481–511. [PubMed: 17376027]

11. Soderling SH, Bayuga SJ, Beavo JA. Identification and characterization of a novel family of cyclic nucleotide phosphodiesterases. J Biol Chem 1998;273:15553–15558. [PubMed: 9624145]

12. Fisher DA, Smith JF, Pillar JS, St Denis SH, Cheng JB. Isolation and characterization of PDE8A, a novel human cAMP-specific phosphodiesterase. J Biol Chem 1998;273:15559–15564. [PubMed: 9624146]

13. Wang P, Wu P, Egan RW, Billah MM. Identification and characterization of a new human type 9 cGMP-specific phosphodiesterase splice variant (PDE9A5) differential tissue distribution and subcellular localization of PDE9A variants. Gene 2003;314:15–27. [PubMed: 14527714]

14. Huai Q, Wang H, Zhang W, Colman RW, Robinson H, Ke H. Crystal structure of phosphodiesterase 9 shows orientation variation of inhibitor 3-isobutyl-1-methylxanthine binding. Proc Natl Acad Sci USA 2004;101:9624–9629. [PubMed: 15210993]

15. McCarty MF. cGMP may have trophic effects on beta cell function comparable to those of cAMP, implying a role for high-dose biotin in prevention/treatment of diabetes. Med Hypotheses 2006;66:323–328. [PubMed: 16309850]

16. Van Staveren WC, Steinbusch HW, Markerink-Van Ittersum M, Repaske DR, Goy MF, Kotera J, Omori K, Beavo JA, De Vente J. mRNA expression patterns of the cGMP-hydrolyzing phosphodiesterases types 2, 5, and 9 during development of the rat brain. J Comp Neurol 2003;467:566–580. [PubMed: 14624489]

17. de Vente J, Markerink-van Ittersum M, Vles JS. The role of phosphodiesterase isoforms 2, 5, and 9 in the regulation of NO-dependent and NO-independent cGMP production in the rat cervical spinal cord. J Chem Neuroanat 2006;31:275–303. [PubMed: 16621445]

18. Diederen RM, La Heij EC, Markerink-van Ittersum M, Kijlstra A, Hendrikse F, de Vente J. Selective blockade of phosphodiesterase types 2, 5 and 9 results in cyclic 3′5′ guanosine monophosphate accumulation in retinal pigment epithelium cells. Br J Ophthalmol 2007;91:379–384. [PubMed: 16943225]

19. Fryburg, DA., et al. Treatment of insulin resistance syndrome and type 2 diabetes with PDE9 inhibitors. WO 03/037432 A1. 2003.

20. Deninno, MP., et al. PDE9 Inhibitors for Treating Cardiovascular Disorders. WO 03/037899. 2003.

21. Bell, AS., et al. PDE9 inhibitors for treating type 2 diabetes, metabokic syndrome, and cardiovasculate disease. WO 2004/096811. 2004.

22. Deninno MP, Andrews M, Bell AS, Chen Y, Eller-Zarbo C, Eshelby N, Etienne JB, Moore DE, Palmer MJ, Visser MS, Yu LJ, Zavadoski WJ, Michael Gibbs E. The discovery of potent, selective, and orally bioavailable PDE9 inhibitors as potential hypoglycemic agents. Bioorg Med Chem Lett 2009;19:2537–2541. [PubMed: 19339180]

23. Black, SC.; Gibbs, EM.; McNeish, JD. Phosphodiesterase 9 inhibition as treatment for obesity-related conditions. WO 2005/041972. 2005.

24. van Staveren WC, Glick J, Markerink-van Ittersum M, Shimizu M, Beavo JA, Steinbusch HW, de Vente J. Cloning and localization of the cGMP-specific phosphodiesterase type 9 in the rat brain. J Neurocytol 2002;31:729–741. [PubMed: 14501210]

25. Hendrix, M., et al. 6-Arylamino-5-cyano-4-pyrimidinones as PDE9A inhibitors. WO 2004/113306. 2004.

26. Reyes-Irisarri E, Markerink-Van Ittersum M, Mengod G, de Vente J. Expression of the cGMP-specific phosphodiesterases 2 and 9 in normal and Alzheimer's disease human brains. Eur J Neurosci 2007;25:3332–3338. [PubMed: 17553001]

27. van der Staay FJ, Rutten K, Bärfacker L, Devry J, Erb C, Heckroth H, Karthaus D, Tersteegen A, van Kampen M, Blokland A, Prickaerts J, Reymann KG, Schröder UH, Hendrix M. The novel selective PDE9 inhibitor BAY 73–6691 improves learning and memory in rodents. Neuropharmacology 2008;55:908–918. [PubMed: 18674549]

28. Reneerkens OA, Rutten K, Steinbusch HW, Blokland A, Prickaerts J. Selective phosphodiesterase inhibitors: a promising target for cognition enhancement. Psychopharmacology (Berl) 2009;202:419–443. [PubMed: 18709359]

29. Liu S, Mansour MN, Dillman KS, Perez JR, Danley DE, Aeed PA, Simons SP, Lemotte PK, Menniti FS. Structural basis for the catalytic mechanism of human phosphodiesterase 9. Proc Natl Acad Sci USA 2008;105:13309–13314. [PubMed: 18757755]

30. Wunder F, Tersteegen A, Rebmann A, Erb C, Fahrig T, Hendrix M. Characterization of the first potent and selective PDE9 inhibitor using a cGMP reporter cell line. Mol Pharmacol 2005;68:1775–1781. [PubMed: 16150925]

31. Ke H, Wang H. Crystal structures of phosphodiesterases and implications on substrate specificity and inhibitor selectivity. Curr Top Med Chem 2007;7:391–403. [PubMed: 17305581]

32. Huai Q, Colicelli J, Ke H. The crystal structure of AMP-bound PDE4 suggests a mechanism for phosphodiesterase catalysis. Biochemistry 2003;42:13220–13226. [PubMed: 14609333]

33. Wang H, Liu Y, Huai Q, Cai J, Zoraghi R, Francis SH, Corbin JD, Robinson H, Xin Z, Lin G, Ke H. Multiple conformations of phosphodiesterase-5: implications for enzyme function and drug development. J Biol Chem 2006;281:21469–21479. [PubMed: 16735511]

34. Wang H, Robinson H, Ke H. The molecular basis for recognition of different substrates by phosphodiesterase families 4 and 10. J Mol Biol 2007;371:302–307. [PubMed: 17582435]

35. Wang H, Ye M, Robinson H, Francis SH, Ke H. Conformational variations of both PDE5 and inhibitors provide the structural basis for the physiological effects of vardenafil and sildenafil. Mol Pharmacol 2008;73:104–110. [PubMed: 17959709]

36. Wang H, Yan Z, Yang S, Cai J, Robinson H, Ke H. Kinetic and Structural Studies of Phosphodiesterase-8A and Implication on the Inhibitor Selectivity. Biochemistry 2008;47:12760–12768. [PubMed: 18983167]

37. Otwinowski Z, Minor W. Processing of X-ray diffraction data collected in oscillation mode. Methods Enzymol 1997;276:307–326.

38. Navaza J, Saludjian P. AMoRe: an automated molecular replacement program package. Methods Enzymol 1997;276:581–594.

39. Jones TA, Zou JY, Cowan SW, Kjeldgaard M. Improved methods for building protein models in electron density maps and the location of errors in these models. Acta Cryst 1991;A47:110–119.

40. Brünger AT, Adams PD, Clore GM, DeLano WL, Gros P, Grosse-Kunstleve RW, Jiang JS, Kuszewski J, Nilges M, Pannu NS, Read RJ, Rice LM, Simonson T, Warren G. L Crystallography and NMR system: A new software suite for macromolecular structure determination. Acta Cryst 1998;D54:905–921.
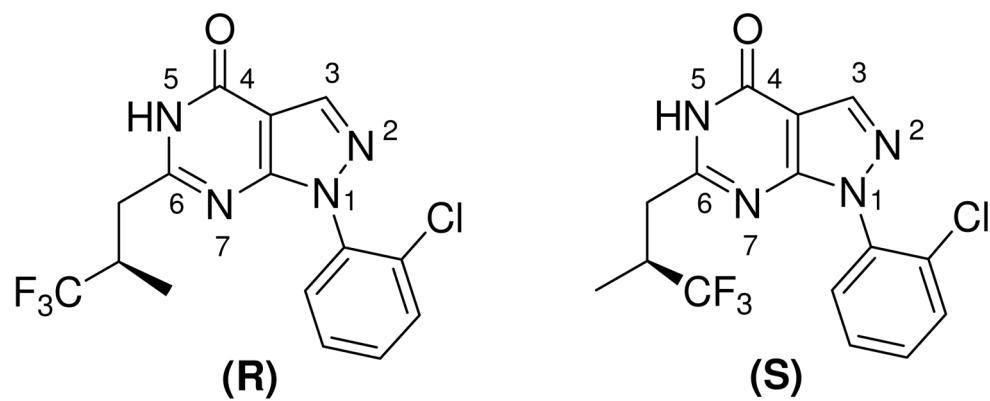
Fig. 1.
Chemical structure of PDE9 inhibitor 1-(2-chlorophenyl)-6-(3,3,3-trifluoro-2-methylpropyl)-1*H*-pyrazolo[3,4-*d*]pyrimidine-4(5*H*)-one (**1**).

(A)   **(B)**

(C)   (D)
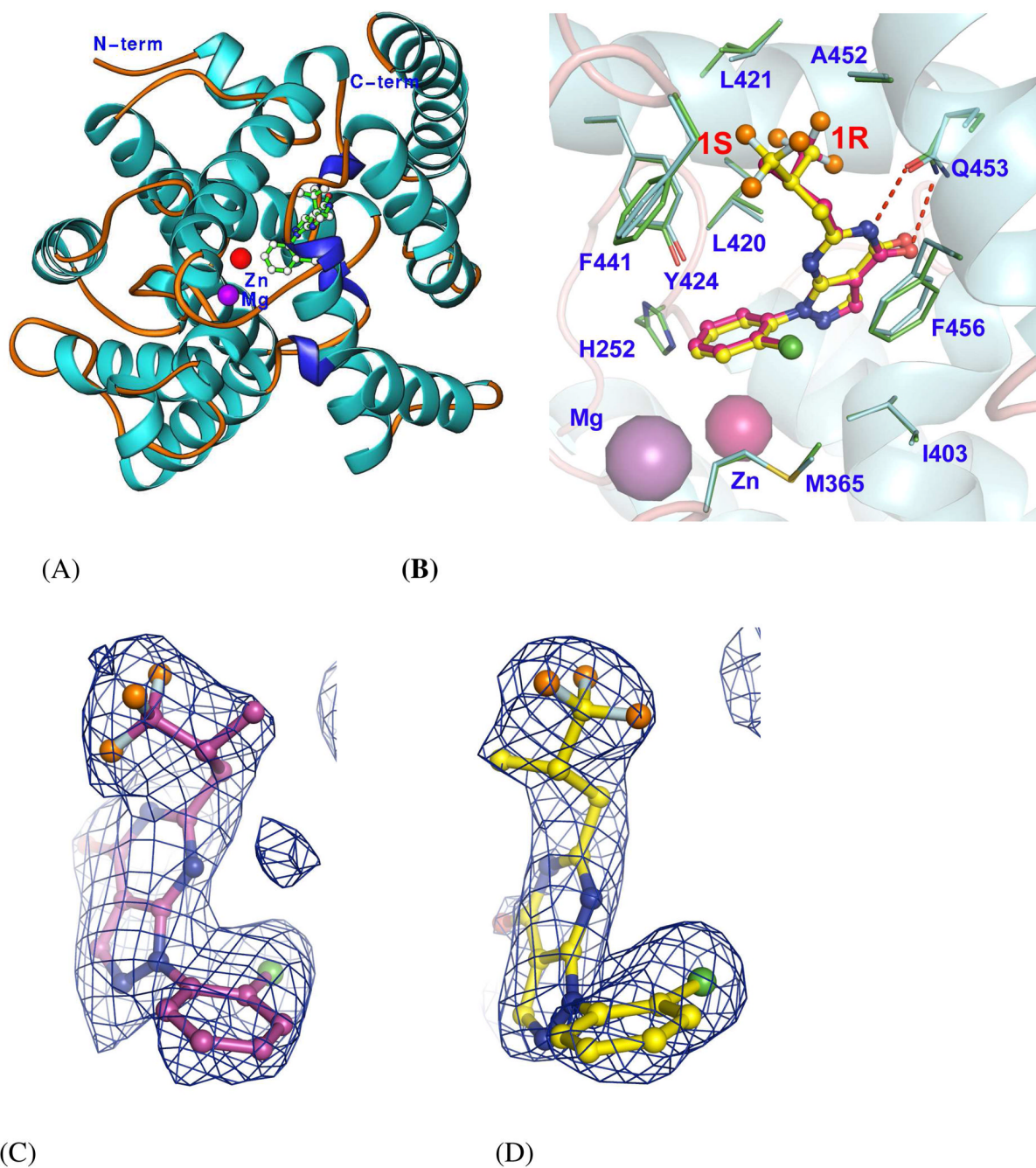
Fig. 2.
Structures of the PDE9A-**1** complexes. (A) Ribbon diagram of the PDE9A2 catalytic domain.
(B) Superposition of the binding of **1r** (yellow bonds) over **1s** (pink bonds). The binding
residues of PDE9A (green and cyan bonds) have similar conformations. The dotted lines
represent the hydrogen bonds between Gln453 and inhibitor **1**. The colors for atoms of **1** are:
orange for fluorine, green for chlorine, blue for nitrogen, and red for oxygen. (C) and (D)
Electron density for **1r** and **1s**. The (Fo-Fc) maps were calculated from the structures with
omission of the inhibitors and contoured at 3 sigmas.
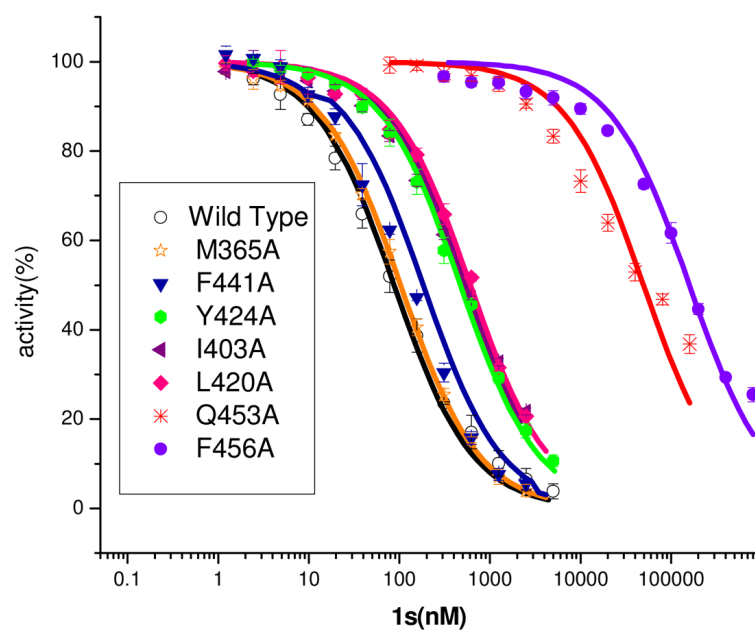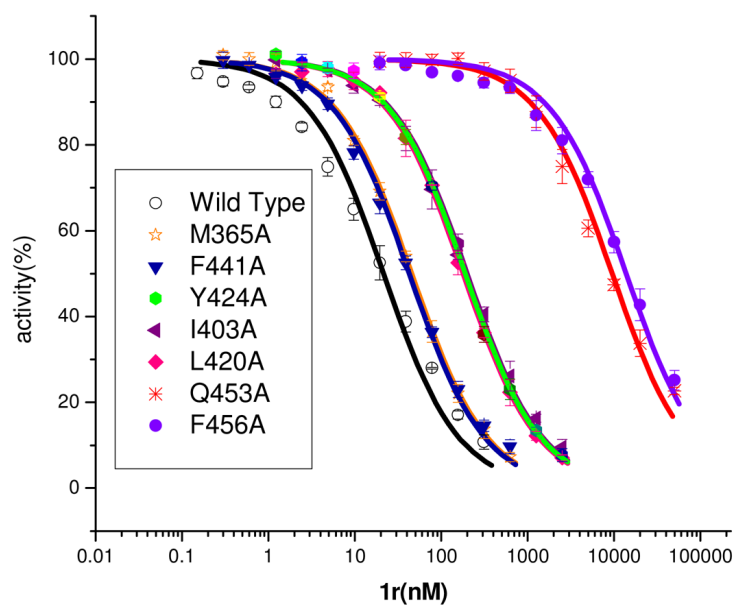
Fig. 3.
Inhibition of the wildtype PDE9A catalytic domain and its mutants by inhibitors **1r** and **1s**.

(A)   (B)   (C)
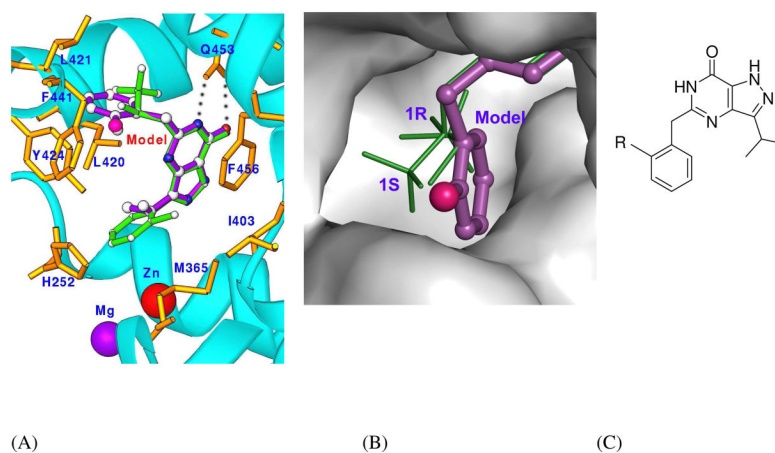
Fig. 4.
Docking of a model compound to the active site of PDE9A. (A) A comparison of the modeled compound (pink bonds) with **1r** (green bonds). The binding residues of PDE9A are in the golden color. The dotted lines represent the hydrogen bonds between Gln453 and O_4 and N5 of the inhibitors. The small pink ball of the model compound represents a potential substitution group that points towards the open molecular surface and could be varied to obtain the best affinity. (B) Surface presentation of the subpocket for binding of trifluomethyl groups of **1r** and **1s**. (C) Chemical structure of the model compound.

Table 1

Statistics on diffraction data and structure refinement

Data collection	PDE9-1r	PDE9-1s
Space group	$P4_12_12$	$P4_12_12$
Unit cell (*a, c*, Å)	103.2, 270.8	103.3, 271.1
Resolution (Å)	2.7	2.5
Total measurements	453,044	578,551
Unique reflections	41,185	51,787
Completeness (%)	100.0 (100.0)[*]	99.9(100.0)[*]
Average I/σ	12.2 (4.8)[*]	12.6 (4.8)[*]
Rmerge	0.084 (0.59)[*]	0.081 (0.57)[*]
Structure Refinement		
R-factor	0.230	0.223
R-free	0.258 (10.0%)[‡]	0.245
Resolution (Å)	15–2.7	15–2.5
Reflections	39,257	49,441
RMS deviation for		
Bond	0.007 Å	0.007
Angle	1.3°	1.2°
Average B-factor (Å²)		
Protein	57.4 (5264)[§]	51.5 (5288)
Inhibitor	45.7 (48)	44.9 (48)
Zn	46.0 (2)	53.5 (2)
Mg	43.5 (2)	37.6 (2)
Water	39.7 (16)	36.2 (16)

[*] The numbers in parentheses are for the highest resolution shell.

[‡] The percentage of reflections omitted for calculation of R-free.

[§] The number of atoms in the crystallographic asymmetric unit.

Table 2

Alignment of inhibitor binding residues in the PDE families

	251*	252	365	403	405*	406*	413*	417*	420	421	424	441	452	453	456	460*
PDE9A	F	H	M	I	N	E	A	V	L	L	Y	F	A	Q	F	V
PDE5A	Y	H	L	L	A	I	Q	A	V	A	F	M	M	Q	F	I
PDE6A	Y	H	L	L	A	I	Q	A	V	A	F	M	L	Q	F	V
PDE10A	Y	H	L	L	S	V	T	A	I	Y	F	M	G	Q	F	V
PDE1B	Y	H	M	I	H	P	H	T	L	M	F	L	S	Q	F	I
PDE2A	Y	H	L	L	D	Q	T	A	I	Y	F	M	L	Q	F	I
PDE3B	Y	H	L	I	G	P	H	T	I	V	F	F	L	Q	F	I
PDE11A	Y	H	L	L	A	V	S	A	V	T	F	F	L	Q	W	I
PDE4D	Y	H	M	L	N	P	Y	T	I	M	F	M	S	Q	F	I
PDE7A	Y	H	I	I	N	P	S	S	V	T	F	L	I	Q	F	W
PDE8A	Y	H	M	V	N	P	C	A	I	S	Y	Y	S	Q	F	F

Residues with symbol * are located in a 4.5 Å radius to the inhibitors and are not normally claimed as the binding residues, but may be useful for design of new inhibitors.

Table 3

Inhibition of PDE9 and its mutants by inhibitors **1r** and **1s**

Proteins	IC$_{50}$ (nM) 1s	IC$_{50}$ (nM) 1r
wildtype	88±17	22±3
L420A	607±31	179±17
Y424A	471±19	190±10
F456A	159±9×10^3	14±2×10^3
Q453A	50±5×10^3	9.6±1.3×10^3
M365A	103±6	46±4
F441A	129±9	43 ± 1
I403A	519±26	200±25